ROLE OF NONDESTRUCTIVE EVALUATION FOR THE PURPOSE OF THE UNDERSTANDING FRACTURE MECHANISM

Y. J. Park[1*], M. Enoki[1], T. Suga[2] and T. Kishi[3]

[1]Department of Materials Science, School of Engineering, The University of Tokyo
7-3-1 Hongo, Bunkyo-ku, Tokyo 113-8656, Japan
[2]Research Center for Advanced Science and Technology, The University of Tokyo
4-6-1 Komaba, Meguro-ku, Tokyo 153-8904, Japan
[3]National Institute for Material s Science, 1-2-1 Sengen, Tsukuba, Ibaraki 305-0047, Japan

ABSTRACT
The bonded area is largely affected by the surface morphology and mechanical properties of materials by surface activated bonding (SAB) process, because the room temperature bonding process is carried out under a low temperature and low pressure for short time. Accordingly, interfacial defects cause fatally harmful problems in many cases. For an application of this technique, it is important to know the effect of interfacial defects on fracture behavior. The fracture mechanism and its criterion for the growth of interfacial defects were investigated using the Al/Sapphire joint. It became clear that the growth of interfacial defects is the dominant factor for crack propagation. An estimation of stress intensity factor for the growth of interfacial defects was tried in two ways, stress criterion and energy criterion. A critical stress intensity factor for the growth of interfacial defects was estimated as 0.3-0.5MPam$^{1/2}$ by the analysis of FEM calculation and experimental observation.

KEYWORD room temperature bonding, interfacial fracture, fracture criterion, FEM

INTRODUCTION

With the traditional method of joining the metals, semiconductors and ceramics, diffusion and reaction driven by heat at high temperature provided bonding with the joint [1-3]. Some harmful effects due to the process involving heating, such as the generation of residual thermal stress [2,4] and the formation of brittle reaction products [3,5] at the interface region, on mechanical and functional property have been noticed as the barrier for the application.
In recent years, a novel method of Surface Activated Bonding (SAB) was invented [6-8] and its engineering importance is now being emphasized. The basic concept underlying this technique is that two atomically clean solid surfaces under contact show a strong adhesive force [9]. The surface exposed to ambient atmosphere is covered with oxides and adsorbed layers. By means of sputtering or radical beam treatment in an ultra high vacuum, impurity layers are removed so that a clean surface emerges. Therefore, direct bonding at atomic level is acquired between high-energy state pure surfaces. Because work of adherence between dissimilar solid materials is positive except in extremely rare cases, it is regarded that bonding is achieved only if they are in intimate contact of atomic bonding distance.
The SAB process brought about innovative benefits because all the processes are carried out under low temperature and pressure. That is, this technology is free from the interfacial problems pointed out at high temperature and also enables to bond electronic devices that are not allowed to be heated.
Until now, research activities have been concentrated on the study of the bonding mechanism and on the investigation into the factors affecting mechanical properties. On the theoretical side, calculations of atomic and electronic structures of interfaces indicating the bonding type have been fruitful [10,11]. There have been the rigorous attempts to understand the phenomena of frictional adherence under high vacuums, like space [6,9,12]. On the other hand, the report was restricted to the results of joint strength as a function of bonding conditions [7,8]. Consequently the situation is that the knowledge on fracture mechanism and its criterion are almost unknown. From the comparison between measured bonded area and finite element method (FEM) simulated one for Al/Sapphire system, authors have already made clear the process of contact deformation in a quantitative manner [13]. Bonded area is largely affected by the surface morphology and mechanical properties of materials, because the SAB process is carried out under a low temperature and pressure for a short time. Accordingly, it can be generally stated that the existence of interfacial defects (unbonded parts) is an unavoidable problem. And moreover, it is already known that the mechanical properties of bonded materials, such as fracture behavior and fracture energy, depend on the bonded area to a great extent [14].
It is commonly agreed that elucidation of the effect of interfacial defects on fracture behavior is the most necessary task for an application of this technology. In this research, fracture mechanism and its criterion of Al/sapphire joint were investigated by a fracture mechanical approach.

FABRICATION OF SPECIMEN AND TEARING-OFF TEST

Polycrystalline aluminum of 99.5% (2nine) and 99.999% (5nine) purity and c-plane cut sapphire are selected as a model system. Aluminum is known by all-purpose material for SAB joint owing to good bonding for both metal and ceramic. And through the transparent sapphire, bond interface can be observed by CSLM (confocal scanning laser microscope, model 1LM21H, Lasertech Co.). An aluminum foil of 1μm thickness was inserted to provide a precrack, and pressures of 20 MPa and 40MPa were applied to get joint. All the processes were conducted under ultra high vacuum of 10^{-7}Pa or more. Bonded interface is square rectangle of 5x5 mm^2. Shape of specimen and confirmation of precrack is shown in Fig. 1. Details of fabrication process and instruments are available in another paper [13].

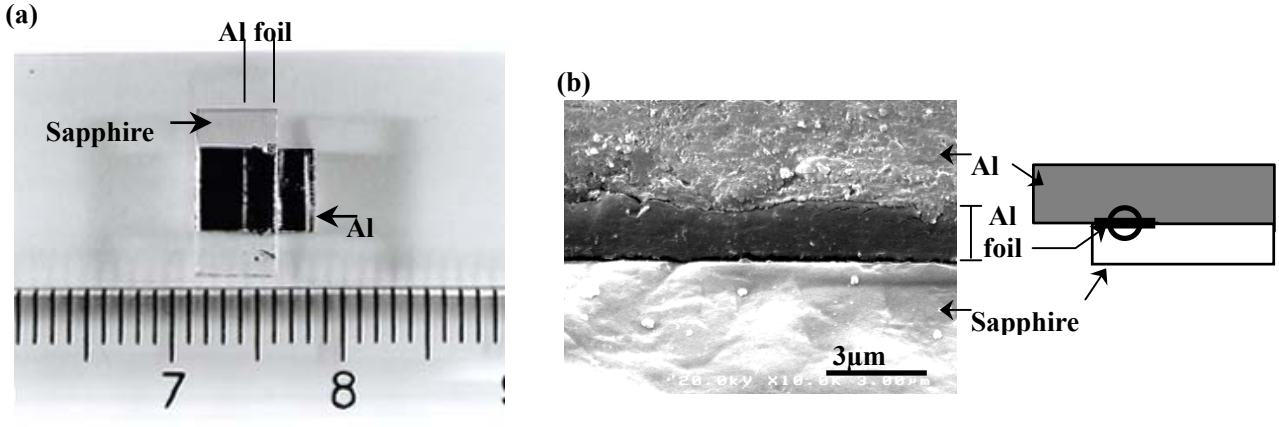

Figure 1 Shape of Tearing-Off Test Specimen Fabricated by SAB Process
(a) top view of specimen (b) cross section view of precrack

The tearing-off test was conducted in the following way. After fixing the sapphire part, the protruded part of aluminum was pulled up at constant speed of 0.1mm/min for propagation of precrack. During the crack propagation, real time observation was made using a video-microscope. Both load and length within which interfacial defect grows are given from this monitoring. Crack front of unloaded specimen and fracture surface were observed by CSLM and SEM, respectively.

ESTIMATION OF STRESS INTENSITY FACTOR FOR THE INTERFACIAL DEFECT

The criterion for the growth of interfacial defects was derived by the combination of characteristic values of experimental and FEM calculation. Because pure aluminum indicates an elastic-plastic behavior with low yield stress, the stress field at the interface region was calculated by FEM. An estimation of stress intensity factor for the growth of interfacial defect was tried in two ways, one is by stress criterion and the other by energy criterion. The validity of these two approaches is discussed.

For the stress criterion, the stress field at the interface region (σ_i and τ_i) developed by main crack and external load was acquired from the finite element mesh without containing defect element, at first. Calculated values are used as a boundary condition for interfacial defects. Stress intensity factor at interfacial defect is derived from $K=(K_1^2+K_2^2)^{1/2}$ using Eqn. (1)[15].

$$\begin{aligned} K_1 &= \frac{\sqrt{a}}{\cosh \pi\varepsilon}\{\sigma_i\left[\cos(\varepsilon\log 2a) + 2\varepsilon\sin(\varepsilon\log 2a)\right] \\ &\qquad + \tau_i\left[\sin(\varepsilon\log 2a) - 2\varepsilon\cos(\varepsilon\log 2a)\right]\} \\ K_2 &= \frac{\sqrt{a}}{\cosh \pi\varepsilon}\{\tau_i\left[\cos(\varepsilon\log 2a) + 2\varepsilon\sin(\varepsilon\log 2a)\right] \\ &\qquad - \sigma_i\left[\sin(\varepsilon\log 2a) - 2\varepsilon\cos(\varepsilon\log 2a)\right]\} \end{aligned} \tag{1}$$

where a is for radius of penetrated interfacial defect, ε for materials constant which characterizes the compatibility of bimaterial joint and β for Dunders' parameter.

With the energy criterion, J-integral for the growth of interfacial defects was done by VCEM (Virtual Crack Extension Method)[16]. Defect element having radius a is located at the critical distance of d_c from the main crack. According to the SSV (Z.Suo, C.F.Shih and A.G.Varias) model [17,18], an elastic layer of thickness h was introduced to aluminum side (shown in Fig.2). For the comparison, J-integral values are converted into stress intensity factor adopting the following Eqn. (2)[19].

$$G = \frac{1}{16\cosh^2(\varepsilon\pi)}\left(\frac{\chi_1+1}{\mu_1} + \frac{\chi_2+1}{\mu_2}\right)(K_1^2 + K_2^2) \tag{2}$$

where $\chi=3-4\nu$ and μ is shear modulus.

The finite element mesh was constructed by 4-node rectangle of two dimensional plane strain element. The total number of elements was 5400 at maximum. The elements near the interfacial defect were small enough to achieve accurate calculations. The shortest was 1000 times shorter than interfacial defect. To verify the convergence, iterative calculation was conducted from coarse mesh to fine mesh by increasing the number of element. Material size and mechanical properties used as input data for calculation are given in Table 1.

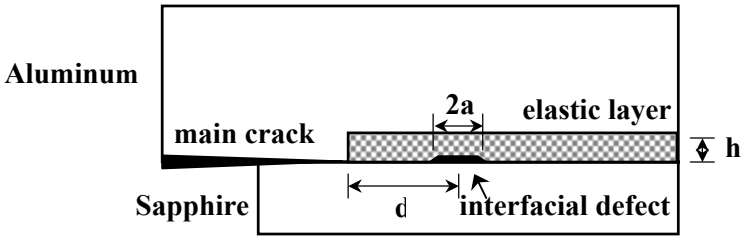

Figure 2 Schematic Illustration for the Concept of SSV Model

Table 1 Conditions for FAB (fast atom beam) Irradiation and Surface Analysis by XPS

FAB conditions		XPS conditions	
FAB source		Stage tilt angle	45 °
acceleration voltage	1.5*kV*	Analysis area	0.8 *mm* dia.
beam current	15*mA*	Vacuum level	3.6-4.5×10^{-8} *Pa*
Vacuum level		Step size	1*eV*
FAB chamber	2.0~3.3×10^{-7} *Pa*	Time/step	20*ms*
(during operation	~2.0×10^{-1} *Pa*)	Repeats	5
transfer chamber	1.1~4.9×10^{-7} *Pa*		
joining chamber	4.0×10^{-7}~9.3×10^{-8} *Pa*		

RESULTS AND DISCUSSION

The interfacial structure of as-bonded joint was observed through transparent sapphire (shown in Fig.3) and the distribution of defect size was obtained (shown in Fig.4). With aluminum 2nine, interfacial defects are originated from the etch-pit of the second phase, which existed originally. The maximum defect size is about 30μm. Distribution of defect size is characterized as small sized high frequency compared with that of aluminum 5nine joint. In the case of Al 5nine-bonded at 20MPa, which is lower than yield strength of used aluminum, bonded and unbonded region alternate periodically. Defect size ranged from 10μm to 100μm. On the other hand, the specimen bonded at high pressure of 40MPa showed a bonded area of 95% or more and the strength of the joint was strong enough to cause a fracture not in the interface but in the sapphire side. Crack propagation occurred in Al 2nine-bonded at 40MPa and Al 5nine-bonded at 20MPa. Thus, results are reported about

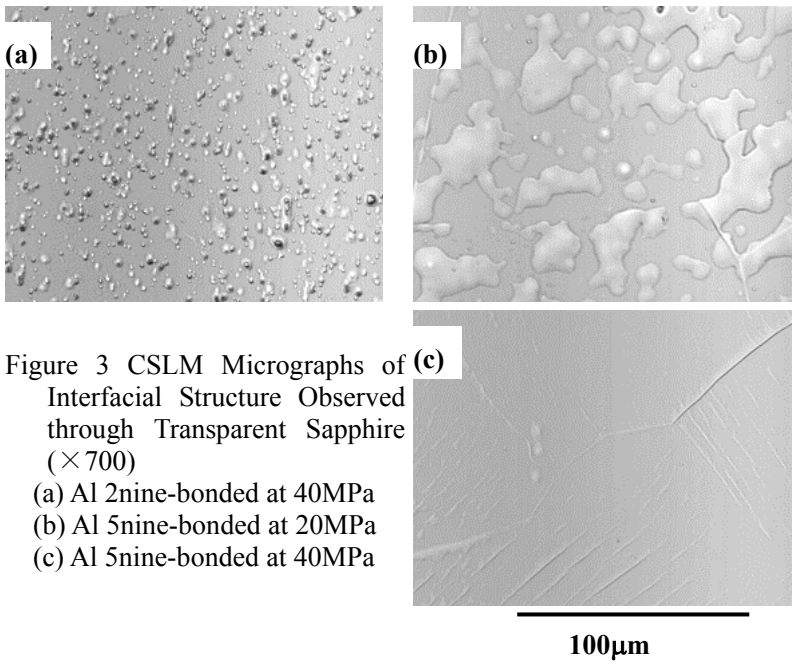

Figure 3 CSLM Micrographs of Interfacial Structure Observed through Transparent Sapphire (×700)
(a) Al 2nine-bonded at 40MPa
(b) Al 5nine-bonded at 20MPa
(c) Al 5nine-bonded at 40MPa

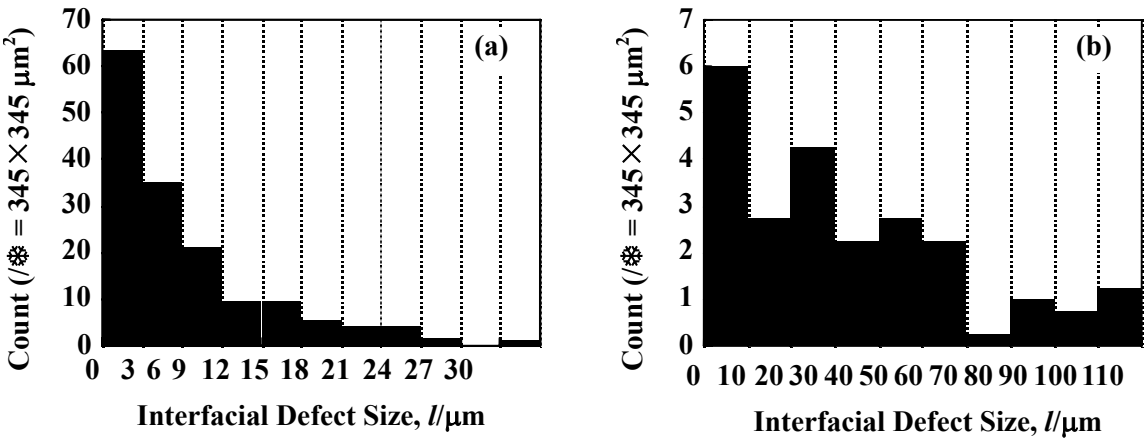

Figure 4 Distribution of Interfacial Defect Size
(a) Al 2nine-bonded at 40MPa (b) Al 5nine-bonded at 20MPa

these two cases below.

In order to investigate defect growth behavior more precisely, CSLM observation of crack front in unloaded specimen was made (shown in Fig.5). The main crack and propagating direction are marked in the figure. The growth of interfacial defects is clearly seen in the front region of the main crack in both joints. In case of Al 5nine-bonded at 20MPa, round circled island like parts surrounded by grown interfacial defects are still bonded. Blunting of interfacial defect after growth is recognized by a ripple pattern contrast on CSLM and fracture surface morphology on SEM. At these parts, not interfacial fracture but ductile fracture of bonded aluminum is expected at the next step. Figure 6 is a low magnified in-situ observation of loaded specimen and the area of white contrast represents the growing interfacial defects. Reaching maximum load, the main crack begins to propagate. Therefore, we could distinguish the crack propagation from the defect growth. In this paper, the length of this zone is defined as a critical length d_c. They were measured as 200μm and 330μm for Al 2nine-bonded at 40MPa and Al 5nine-bonded at 20MPa, respectively.

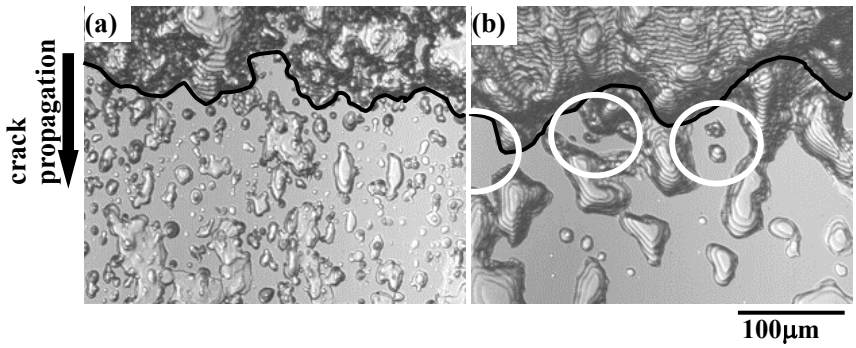

Figure 5 In-Situ Observation of Crack Propagation through Transparent Sapphire (CSLM x700)
(a) Al 2nine-bonded at 40MPa (b) Al 5nine-bonded at 20MPa

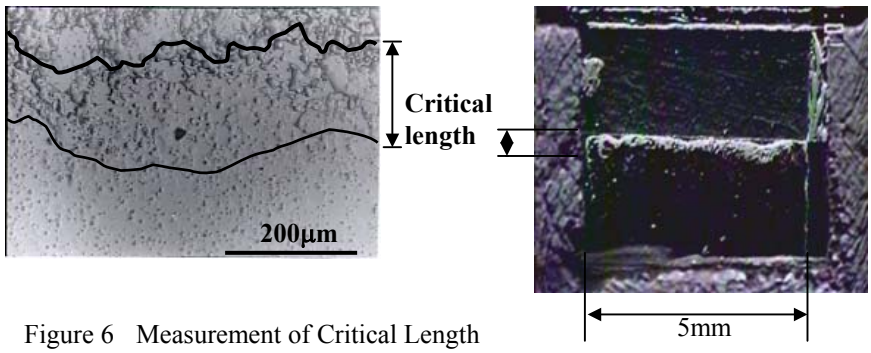

Figure 6 Measurement of Critical Length
(a) Al 2nine-bonded at 40MPa (b) Al 5nine-bonded at 20MPa

From the SEM micrographs of fracture surfaces, crack path can be inferred (shown in Fig.7). Fig.7 (a) is for aluminum-side of Al 2nine-bonded at 40MPa. On the matching surface of sapphire, any traces of aluminum attached were not recognized, so that crack propagated along the interface. Here it is noticeable that defects smaller than 10μm (arrowed) did not grow and defined as a critical defect size. Fig.7 (b) is for aluminum-side of Al 5nine-bonded at 20MPa and aluminum was attached on the matching surface of sapphire, as shown in Fig.7(c). Furthermore, the area of aluminum attached is smaller than that of as-bonded joint, that means the growth of interfacial defects. For Al 5nine-bonded at 20MPa, determination of critical defect size on the fracture surface was not so easy.

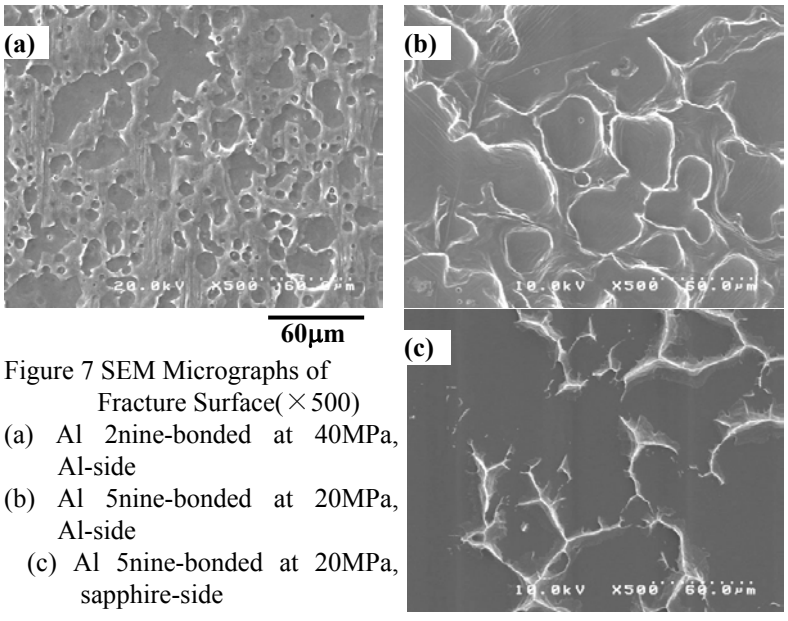

Figure 7 SEM Micrographs of Fracture Surface(×500)
(a) Al 2nine-bonded at 40MPa, Al-side
(b) Al 5nine-bonded at 20MPa, Al-side
(c) Al 5nine-bonded at 20MPa, sapphire-side

As is already known with the ductile metal-ceramic joint without brittle interphase, the propagation of the main crack itself is impossible owing to the blunting [20]. However, interfacial defects were allowed to grow in this research, which resulted in the apparent crack propagation. This fracture mechanism was also ascertained by nondestructive evaluation method using AE source characterization [21].

It became clear that the growth of interfacial defects is a dominant factor in joint fractures. With or without loading mixity, a crack located at the bimaterial interface undergoes mixed mode fracture due to the difference in an elastic modulus [22]. The fracture mechanical approach to the growth of interfacial defects is discussed in the remaining parts of this paper.

The stress intensity factor for the penetrated defect (see Eqn. (1)) and penny shaped defect (see Eqn. (3) [23]) were plotted in Fig. 8.

$$K_1 + i\,K_2 = 2\sigma_i\sqrt{a}\,\Gamma(2 + i\varepsilon) / \Gamma(1/2 + i\varepsilon) \qquad (3)$$

Defects were located at the critical length of 200μm for Al 2nine-bonded at 40MPa and the stress field used as boundary condition was calculated at the load of crack propagation. For the defects of smaller than 30μm, maximum defect size, stress intensity factor showed almost the same dependency on the defect size. According to these results and for the convenience of constructing the mesh, two-dimensional analysis was carried out with the assumption of interfacial penny shaped defect as penetrated defect.

Table 2 Properties and Size of Materials

Al (HT2)	Sapphire
Polycrystal (99.999%) Specimen size $5\times7\times3$ mm^3 Yieldstress 30*Mpa* Work-hardening ($\sigma=k\varepsilon^n$) k=179 *MPa* n=0.4	Single crystal (c-plane) Specimen size $5\times10\times1$ mm^3 Treated as rigid

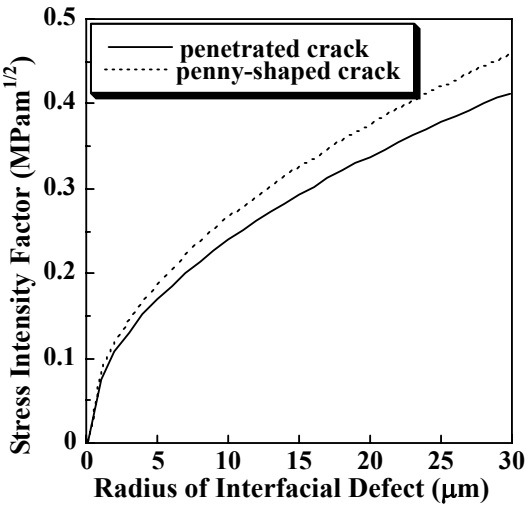

Figure 8 Stress Intensity Factor for the Interfacial Defects of Al 2nine Located at the Critical Length of 200μm

For the stress criterion, stress intensity factor on interfacial defects was calculated on the basis of characteristic values of experimental and stress field at crack propagation load. The characteristic values and measurement conditions are summarized in Table 2. The stress intensity factor for several sizes of interfacial defects was plotted as a function of a distance from the main crack. For Al 2nine-bonded at 40MPa (Fig.9 (a)), critical stress intensity factor was estimated as 0.3MPam$^{1/2}$ from the critical defect size (a=5μm). A predicted critical length of 200μm, by the critical stress intensity factor and maximum defect size (a=15μm), shows good agreement with the experimentally measured one. A similar result was acquired in the case of Al 5nine-bonded at 20MPa (Fig.9 (b)). Growth of interfacial defects by debonding was restricted to a certain amount and ductile fracture of still bonded aluminum followed. The reason for a change in the crack path is ascribed to the decreased stress intensity factor caused by the blunting of grown defect as mentioned before. The height of interfacial defects in as-bonded state was about 1μm, while that of growth stopped was measured about 5μm or more.

Because the Eqn. (1) used here is an analytic solution of elastic mechanics, its application to the Al/Sapphire system

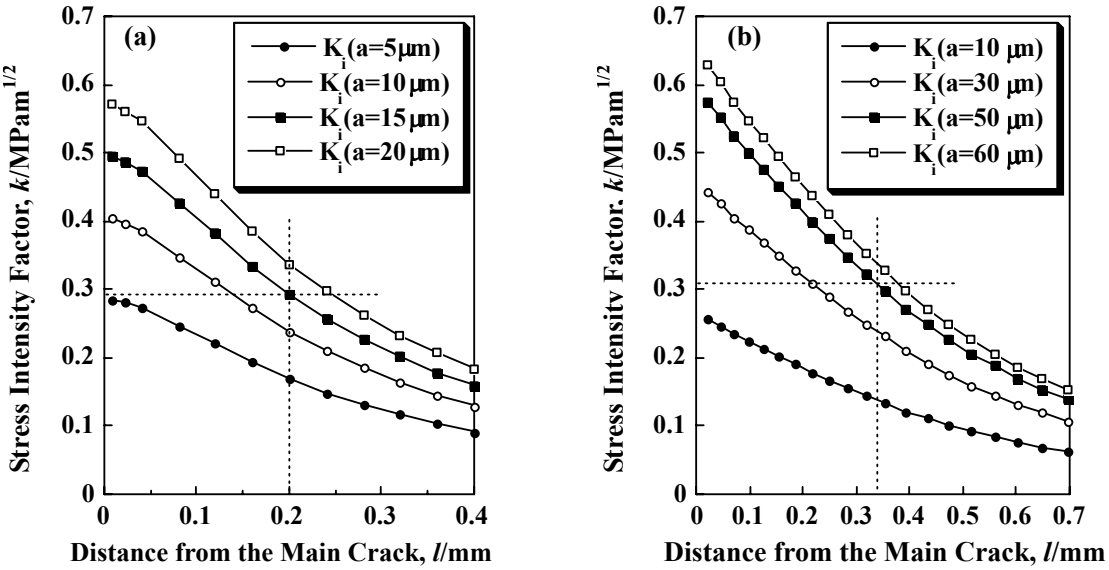

Figure 9 Determination of Critical Stress Intensity Factor for the Growth of Interfacial Defect by Stress Criterion (a) Al 2nine-bonded at 40MPa (b) Al 5nine-bonded at 20MPa

exhibiting elastic-plastic behavior should be doubted. However, the appropriateness of this equation was verified from the calculated results that the dimension of von Mises yield region is smaller than the critical length of this research (shown in Fig.10). Consequently, it is rational to apply Eqn. (1) for interfacial defect located at critical length.

In the course of J-integral adopting the SSV model, an elastic layer at aluminum side along the interface has the same elastic modulus and Poisson ratio. This layer came from the knowledge of a mean distance among the dislocations of material [17]. That is, the area within distance h from the interfacial defect can be treated as elastic, because there are no dislocations. Thickness h is known as 0.1-1μm. Another hypothesis to explain the existence of this layer is the phenomena of crack propagation along the bimaterial interface of ductile metal and ceramic, which is possible only if there is sufficient stress concentration built by not blunt interfacial defect [18]. This is true with this paper. While the main crack became blunt to be stationary, interfacial defects showed a certain amount of growth before they were stopped.

Preliminary calculation of stress field revealed little difference between 1μm and 10μm thick elastic layer. For convenience in constructing the mesh and concerning the previous results, thickness of elastic layer was assumed as 10μm.

Figure 11 represents the results of J-integral performed near the interfacial defects. Amount of released energy, J value, increases as applied external load increases. On the other hand, J value shows the maximum at an intermediate size of interfacial defect for constant external load. Results having same tendency were reported in the simulation of tensile loading for metal/rigid joint [18]. Critical energy release rate, J_c, is obtained at the maximum defect size and fracture load. That value ranged 1.3-2.3J/mm^2 and is smaller than the fracture energy of sapphire, 12J/mm^2. It is consistent with our previous finding that the process of defect growth is nothing but an interfacial debonding. Stress intensity factor converted from energy release rate is given in Fig. 12.

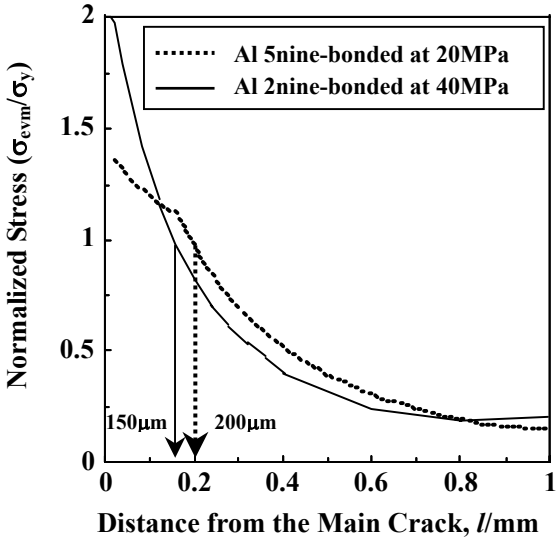

Figure 10 Calculated Length of Small Scale Yielding Zone by Equivalent von Mises Stress at the Interfacial Region

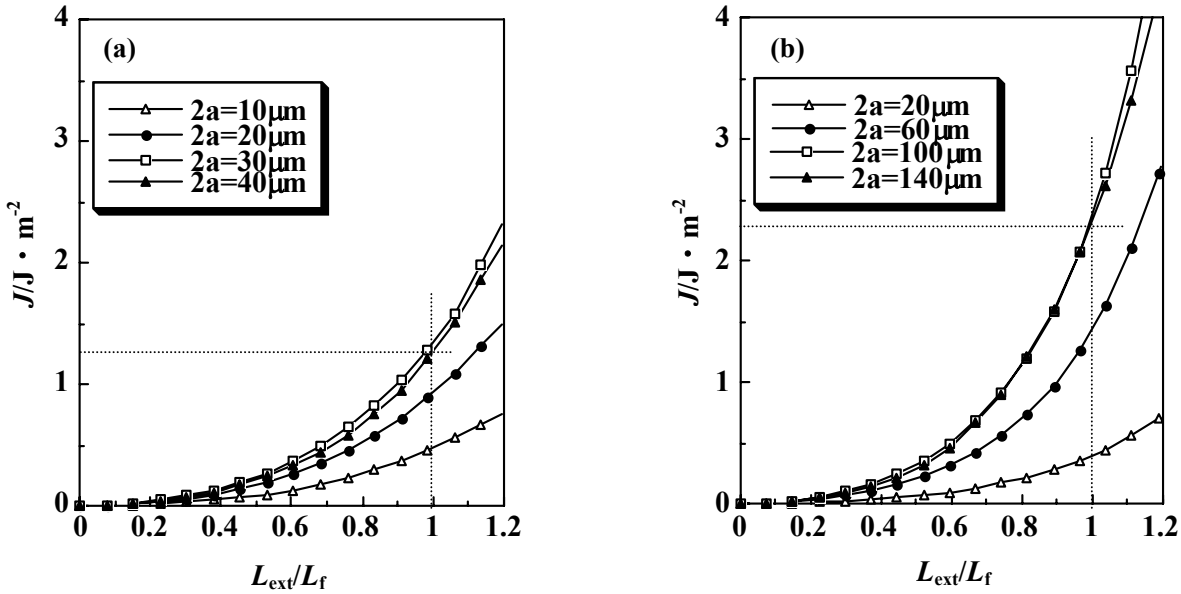

Figure 11 Calculation of J-Integral by VCEM for Interfacial Defects Located at the Critical Length
(a) Al 2nine-bonded at 40MPa (b) Al 5nine-bonded at 20MPa
(where, L_{ext}:external load, L_f:fracture load)

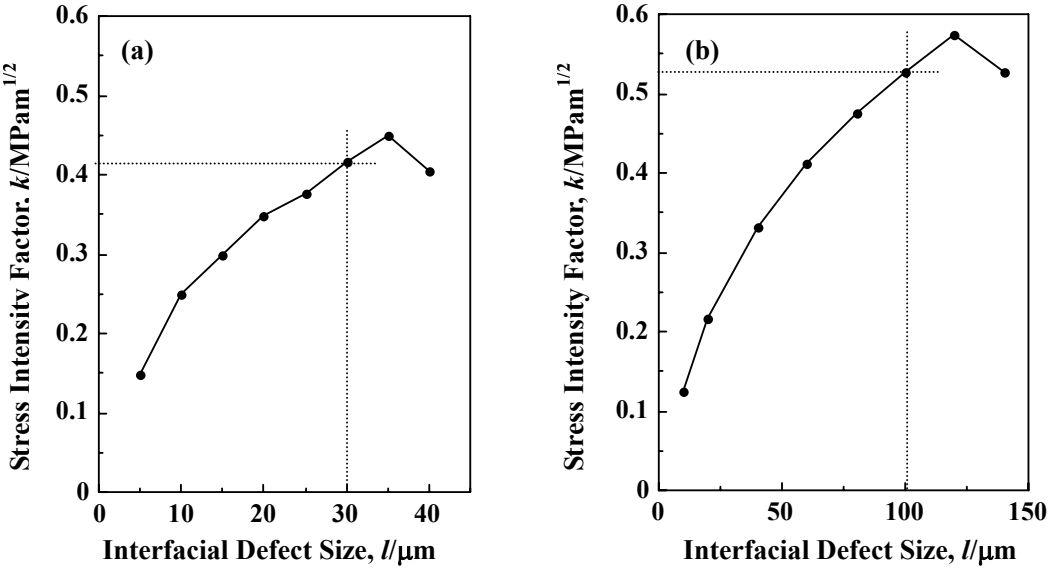

Figure 12 Conversion of Calculated J-Integral Values into Stress Intensity Factor
(a) Al 2nine-bonded at 40MPa (b) Al 5nine-bonded at 20MPa

Critical value is estimated as 0.4MPam$^{1/2}$ for Al 2nine-bonded at 40MPa and 0.5MPam$^{1/2}$ for Al 5nine-bonded at 20MPa,

respectively. They are a little larger than the values obtained by stress criterion. This resulted from the difference in the dealing method of the interaction between the main crack and interfacial defects. That is, energy criterion including that mechanism is thought to be more effective.

CONCLUSIONS

The findings of this research are summarized as following.

1. It became clear that the growth of interfacial defects is a dominant mechanism for the crack propagation. The crack propagated by means of the growth of interfacial defects.
2. The criterion for interfacial defects growth was estimated by the combination of experimental results and FEM calculation.
3. Fracture criterion was approached from two methods, stress intensity criterion and energy criterion. Energy criterion, which takes into account of an interaction between the main crack and interfacial defects, is considered more accurate.

ACKNOWLEDGEMENTS

This study was supported by the “Reversible Interconnection of Dissimilar Materials”, section of the “Research for the Future Program” of the Japan Society for Promotion of Science.

REFERENCES

1. Gibbesch, B and Elssner, G. (1992) *Acta Metall. Mater.* 40, pp. S59-S66.
2. Kirchner, H. P., Conway, J. C. and Segall, A. E. (1987) *J. Am. Ceram. Soc.* 70, pp. 104-109.
3. Elssner, G. and Petzow, G. (1990) *ISIJ Int.* 30, pp. 1011-1032.
4. Yuuki, R. and Xu, J. Q. (1994) *Trans. Jpn. Soc. Mech. Eng.* 60, pp. 2544-2552.
5. Bartlett, A. and Evans, A. G. (1993) *Acta Metall. Mater.* 41, pp. 497-504.
6. Pepper, S. V. (1976) *J. Appl. Phys.* 47, pp. 801-808.
7. Funakubo, H. and Akaike, M. (1982) *J. Japan Inst. Metals* 46, pp.935-943.
8. Suga, T., Takahashi, Y., Takagi, H., Gibbesch, B. and Elssner, G. (1992) *Acta Metall. Mater.* 40, pp. S133-S137.
9. Keller, D. V. (1963) *Wear* 6, pp. 353-365.
10. Kruse, C., Finnis, M. W., Milman, V. Y., Payne, M. C., Vita, A. D. and Gillan, M. J. (1994) *J. Am. Ceram. Soc.* 77, pp. 431-436.
11. Kohyama, M. (1996) *Modeling Simul. Mater. Sci. Eng.* 4, 397-408.
12. Buckley, D. H. (1967) *ASTM Spe. Tech. Pub.* 431, p .248.
13. Park, Y. J., Enoki, M., Suga, T. and Kishi, T. (1999) *J. Japan Inst. Metals* 63, pp.1485-1489.
14. Ohashi, O. and Hashimoto, T. (1976) *J. of JWS* 45, pp. 485-491.
15. Sih, G. C. (1973) *Handbook Stress Intensity Factors, Institute of Fracture and Solid Mechanics*, Lehigh University, Bethlehem, PA, p. 1.8.1.
16. Parks, D. M. (1974) *Int. J. Fract.* 10, pp. 487-502.
17. Suo, Z., Shih, C. F. and Varias, A. G. (1993) *Acta Metall. Mater.* 41, pp. 1551-1557.
18. He, M. Y., Evans, A. G. and Hutchinson, J. W. (1996) *Acta Mater.* 44, pp. 2963-2971.
19. Malyshev, B. and Salganik, R. (1965) *Int. J. Fract. Mech.* pp. 1114-119.
20. Turner, M. R. and Evans, A. G (1996) *Acta Mater.* 44, pp. 863-871.
21. Park, Y. J., Enoki, M., Suga, T. and Kishi, T. (1999) Proc. 9th NDC, Sydney, Australia, pp. 21.
22. Erdogan, F. (1965) *J. Appl. Mech.* 32, pp. 403-411.
23. Kassir, M. K. and Bregman, A. M. (1972) *Trans. ASME, Ser. E, J. Appl. Mech.* 39, pp. 308-310.